Kobirumaki-Shimozawa et al., http://www.jgp.org/cgi/content/full/jgp.201511484/DC1

Supplemental Materials and methods

Vector construction

Recombinant ADVs encoding mouse α-actinin-3-AcGFP (Ad-actinin-AcGFP; GenBank accession no. NM_013456) were constructed by using the AdMax ADV vector creation kit (Microbix Biosystems Inc.) as suggested by the manufacturer. The α-actinin-3 gene was amplified by using PCR with primers designed according to α-actinin-3 cDNA. Then, the α-actinin-3 cDNA was subcloned to pAcGFP-N1 (Takara Bio Inc.) by using XhoI and Asp718. The PCR fragments were synthesized by PCR using the primers fm_NheI-actinin (5′-ATGCTAGCACCATGATGATGGTTATGCAGCCC-3′) and rm_AcGFP-SalI (5′-TATGTCGACTCACTTGTACAGCTCATCCATGC-3′), and cloned into pDC515 entry vector (NheI/SalI). The pDC515-actinin-3-AcGFP entry vector and the ADV genome plasmid (pBHGfrtΔE1,3FLP) were cotransfected into HEK 293 cells (included in the AdMax ADV vector creation kit) with Lipofectamine LTX (Life Technologies). The cells were overlaid on DMEM medium containing 10% bovine serum and 1% agarose, and incubated at 37°C (+5% CO_2). Single plaques in the medium were excited and amplified by reinfection in HEK 293 cells in DMEM medium containing 5% bovine serum until the fifth virus stock had been harvested. The titer of the sixth Ad-actinin-AcGFP was 10^9–10^{10} viral particles per ml.

Purification of ADVs

The ADVs were purified by using the Vivapure AdenoPACK 20 purification kit (Sartorius AG) for injection into the LV of the heart in vivo. First, the elution buffer containing the purified ADVs was replaced with PBS (−) (137 mM NaCl, 2.7 mM KCl, 10 mM Na_2HPO_4, and 1.8 mM KH_2PO_4, pH 7.4). Then, the ADVs were concentrated by ultrafiltration to yield 10^{11}–10^{12} viral particles per ml in PBS (−) using VIVASPIN 15R (Sartorius AG) for 40–50 min at 3,000 rpm. The viral titer was calculated from the absorbance at 260 nm in the 0.1% (wt/vol) SDS solution (containing 10 mM Tris and 1 mM EDTA). The ADVs were stored at −80°C for up to 2 mo.

Microscopic system for imaging

An upright microscope (BX-51WI; Olympus) combined with a Nipkow confocal scanner (CSU21; Yokogawa Electric Co.) and an electron-multiplying CCD (EMCCD) camera (iXon^{EM}+; Andor Technology) were used based on our previously published procedure (Inoue et al., 2013), at a 512 × 170–pixel resolution at a 100-Hz frame rate throughout the study. A water-immersion lens, either 40× (LUMPlanFL N 40 × W; N/A, 0.80; Olympus) or 60× (LUMPlanFL N 60 × W; N/A, 1.00; Olympus), was used for cardiac sarcomere imaging. A 2× lens (XLFluor 2×/340; N/A, 0.14; Olympus) was used to check AcGFP expression in the whole area of the LV. A custom-made swivel base (Lucir Inc.) was placed between the confocal scanner and EMCCD camera to adjust the orientation of a myocyte (i.e., AcGFP-expressing Z-disks perpendicular to the longitudinal axis of the view window). AcGFP-expressing myocytes in the heart were excited by a 488-nm laser light (HPU50211-PFS; Furukawa Electric Co.) that was directly introduced into CSU21 via air propagation. The diameter of the laser beam was controlled by a beam expander consisting of a concave and a convex lens pair in the optical path to adjust the excitation radius at the sample plane, and the beam was focused at the fiber port of CSU21. Accordingly, the resultant fluorescence signals (emission filter, BA510–550; Olympus) were detected. The usefulness of the in vivo nano-imaging microscopic system for anesthetized mice has already been demonstrated by others in the research areas of cancer (Tada et al., 2007; Gonda et al., 2010) and peripheral circulation (Hamada et al., 2011). By counting the number of myocytes in the Z-direction, it was shown that our optics system with the Nipkow confocal unit enabled imaging at the aforementioned spatial and temporal resolution at a depth of up to ∼150 µm in the heart in vivo.

SL analyses

SL was measured by analyzing the fluorescence plot profiles along the longitudinal axis of an AcGFP-expressing myocyte by using ImageJ software (the region of interest [ROI] width, 5 pixels; National Institutes of Health). In brief, the profiles were analyzed using the multi-peak Gaussian fitting with a linear function of offset ($Y = aX + b$), based on the Levenberg–Marquardt algorithm, and the lengths of individual sarcomeres were calculated as the distance between the centers of two adjacent peaks (indicating the positions of the Z-disks; Serizawa et al., 2011; Shintani et al., 2014, 2015). The position of the ROI was adjusted in each image to enable accurate measurement of the length of the same sarcomere throughout the course of the cardiac cycle. To minimize the error in the SL analysis, sarcomeres showing insufficient fluorescence intensity (F.I.) in Z-disks were not included in the data. Likewise, we developed software to expedite the analysis of diastolic and systolic SL: A frequency histogram was plotted against SL based on the data from a myocyte during ∼30 cardiac cycles (300–500 frames used from one myocyte; see Fig. 4 C). Then, the histogram was fitted with two Gaussian functions using the cumulative frequency plot to obtain binning-independent fitting results (see below for details). The diastolic (or systolic) SL was defined as the greater (or lesser) peak position (see Fig. 4 D). In experiments with isolated hearts, SL or the T-tubular distance (i.e., distance between two fluorescence peaks with CellMask Orange) was measured from static images by multi-peak Gaussian fitting (Fig. 3).

Two-peak Gaussian fitting of SL

Frequency distribution plot for SL (mean of five sarcomeres) provided two peak positions independent of the binning width. The curve fitting was performed on the cumulative probability plot of the SL histogram using the combination of two integrals of the normalized Gaussian functions, i.e.:

$$f(x) = \frac{A_1}{\sqrt{2\sigma_1^2\pi}} \int_{-\infty}^{x} \exp\left(-\frac{(t-\mu_1)^2}{2\sigma_1^2}\right) dt + \frac{1-A_1}{\sqrt{2\sigma_2^2\pi}} \int_{-\infty}^{x} \exp\left(-\frac{(t-\mu_2)^2}{2\sigma_2^2}\right) dt,$$

where µ and σ^2 (with subscript numbers) indicate peak positions and distribution variances, respectively. A_1 was set as $0 \le A_1 \le 1$ in the present study. Fitting the frequency distribution plot with this function provided diastolic and systolic SL values as 1.93 ± 0.03 and 1.73 ± 0.07 µm, respectively (see Fig. 4 D).

Effects of thoracotomy on LVP and HR

First, in the 3–8-wk-old BALB/c male mouse anesthetized with ∼2% isoflurane, the abdomen was opened using an electric scalpel (see above), and a small incision (diameter, ∼3 mm) was made in the diaphragm using the scalpel. Then, a catheter (see above) was inserted into the LV through the apex of the heart,

and LVP and ECG were monitored throughout experimentation at 5 kHz under ∼2% isoflurane according to the method described above. After LVP was measured for ∼20 s under the steady-state condition, the mouse was thoracotomized, and LVP was measured again for ∼20 s. Data obtained during one observation, before and after thoracotomy, were averaged for LVP and HR.

Supplemental Discussion

Supplemental Discussion 1

The Nipkow confocal system has been widely used for the imaging of fast-moving objects; however, this system has an intrinsic "pinhole cross-talk" problem (Shimozawa et al., 2013). Namely, fluorescence in defocused image planes passes through neighboring pinholes in the Nipkow disk, thereby generating high background noise. This intrinsic problem appeared in the present study as the low contrast image in the CellMask-labeled myocyte (Fig. 3 C). Therefore, we used ADV and imaged AcGFP-expressing myocytes (surrounded by non-expressing myocytes) to obtain high contrast images.

Supplemental Discussion 2

The myocyte relative to the confocal image plane may result in an overestimation of SL. However, taking into consideration the careful analysis by the group of Bub (Bub et al., 2010; Botcherby et al., 2013) combined with our SL analysis based on the Gaussian fitting, the maximal overestimation would be ∼3% in the present study, because the length of in-focus images in the image plane (i.e., L_{min} in Bub et al., 2010, and Botcherby et al., 2013) was longer than ∼35 µm in all experiments performed (as in, e.g., Figs. 4 B and 6 B). Moreover, our image reconstruction system can maintain L_{min} at a similar level during the cardiac cycle with a variance of less than ∼10% (see Figs. 6 B, S4, and S5). It is therefore safe to consider that the impact of the myocyte angle on SL is nearly negligible in the present experimental settings.

REFERENCES

Botcherby, E.J., A. Corbett, R.A.B. Burton, C.W. Smith, C. Bollensdorff, M.J. Booth, P. Kohl, T. Wilson, and G. Bub. 2013. Fast measurement of sarcomere length and cell orientation in Langendorff-perfused hearts using remote focusing microscopy. *Circ. Res.* 113:863–870. http://dx.doi.org/10.1161/CIRCRESAHA.113.301704

Bub, G., P. Camelliti, C. Bollensdorff, D.J. Stuckey, G. Picton, R.A.B. Burton, K. Clarke, and P. Kohl. 2010. Measurement and analysis of sarcomere length in rat cardiomyocytes in situ and in vitro. *Am. J. Physiol. Heart Circ. Physiol.* 298:H1616–H1625. http://dx.doi.org/10.1152/ajpheart.00481.2009

Gonda, K., T.M. Watanabe, N. Ohuchi, and H. Higuchi. 2010. In vivo nano-imaging of membrane dynamics in metastatic tumor cells using quantum dots. *J. Biol. Chem.* 285:2750–2757. http://dx.doi.org/10.1074/jbc.M109.075374

Hamada, Y., K. Gonda, M. Takeda, A. Sato, M. Watanabe, T. Yambe, S. Satomi, and N. Ohuchi. 2011. In vivo imaging of the molecular distribution of the VEGF receptor during angiogenesis in a mouse model of ischemia. *Blood.* 118:e93–e100. http://dx.doi.org/10.1182/blood-2010-12-322842

Inoue, T., F. Kobirumaki-Shimozawa, T. Kagemoto, T. Fujii, T. Terui, Y. Kusakari, K. Hongo, S. Morimoto, I. Ohtsuki, K. Hashimoto, and N. Fukuda. 2013. Depressed Frank-Starling mechanism in the left ventricular muscle of the knock-in mouse model of dilated cardiomyopathy with troponin T deletion mutation ΔK210. *J. Mol. Cell. Cardiol.* 63:69–78. http://dx.doi.org/10.1016/j.yjmcc.2013.07.001

Serizawa, T., T. Terui, T. Kagemoto, A. Mizuno, T. Shimozawa, F. Kobirumaki, S. Ishiwata, S. Kurihara, and N. Fukuda. 2011. Real-time measurement of the length of a single sarcomere in rat ventricular myocytes: a novel analysis with quantum dots. *Am. J. Physiol. Cell Physiol.* 301:C1116–C1127. http://dx.doi.org/10.1152/ajpcell.00161.2011

Shimozawa, T., K. Yamagata, T. Kondo, S. Hayashi, A. Shitamukai, D. Konno, F. Matsuzaki, J. Takayama, S. Onami, H. Nakayama, et al. 2013. Improving spinning disk confocal microscopy by preventing pinhole cross-talk for intravital imaging. *Proc. Natl. Acad. Sci. USA.* 110:3399–3404. http://dx.doi.org/10.1073/pnas.1216696110

Shintani, S.A., K. Oyama, F. Kobirumaki-Shimozawa, T. Ohki, S. Ishiwata, and N. Fukuda. 2014. Sarcomere length nanometry in rat neonatal cardiomyocytes expressed with α-actinin–AcGFP in Z discs. *J. Gen. Physiol.* 143:513–524. http://dx.doi.org/10.1085/jgp.201311118

Shintani, S.A., K. Oyama, N. Fukuda, and S. Ishiwata. 2015. High-frequency sarcomeric auto-oscillations induced by heating in living neonatal cardiomyocytes of the rat. *Biochem. Biophys. Res. Commun.* 457:165–170. http://dx.doi.org/10.1016/j.bbrc.2014.12.077

Tada, H., H. Higuchi, T.M. Wanatabe, and N. Ohuchi. 2007. In vivo real-time tracking of single quantum dots conjugated with monoclonal anti-HER2 antibody in tumors of mice. *Cancer Res.* 67:1138–1144. http://dx.doi.org/10.1158/0008-5472.CAN-06-1185

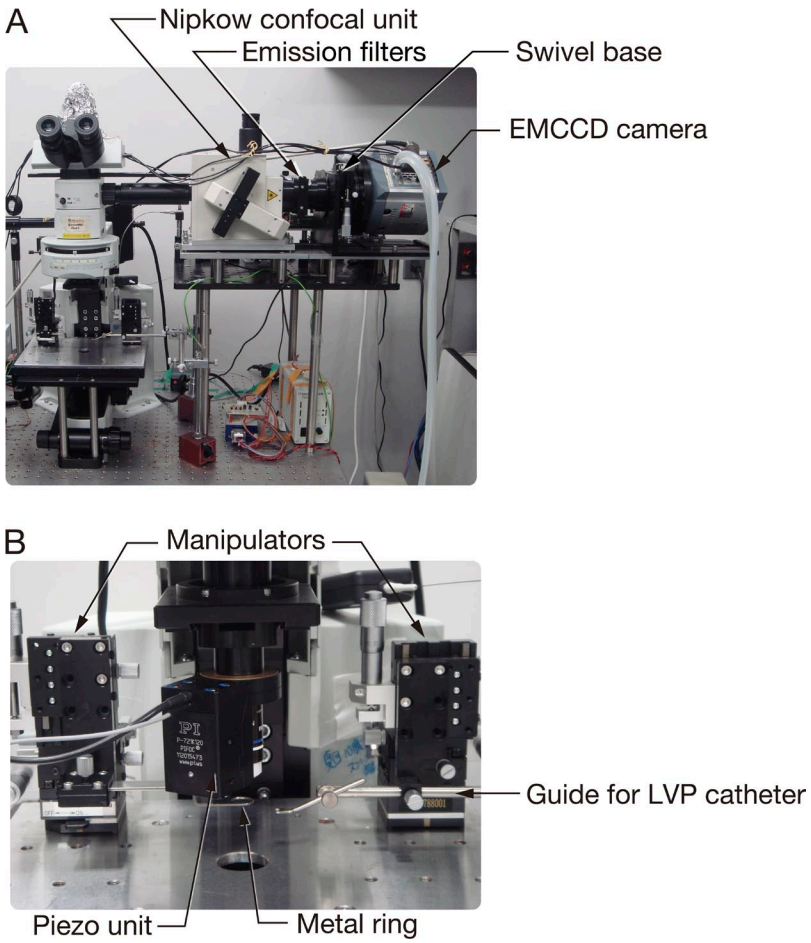

Figure S1. In vivo cardiac sarcomere imaging system. (A) The microscopic system consisting of a Nipkow confocal unit, an EMCCD camera, and a piezo objective lens positioner. A custom-made swivel base was placed between the confocal scanner and EMCCD camera to adjust the orientation of myocytes in the view window (see Fig. 1 A). The emission filters were placed between the confocal scanner and swivel base. (B) Close-up view of the stage of the microscope. The piezo unit was placed on the base of the objective lens (see Fig. 6 and Materials and methods). The micro-manipulator on the left was used to hold the metal objective ring described in Fig. 1 A. Similarly, the micro-manipulator on the right was used to hold the metal guide for the LVP catheter.

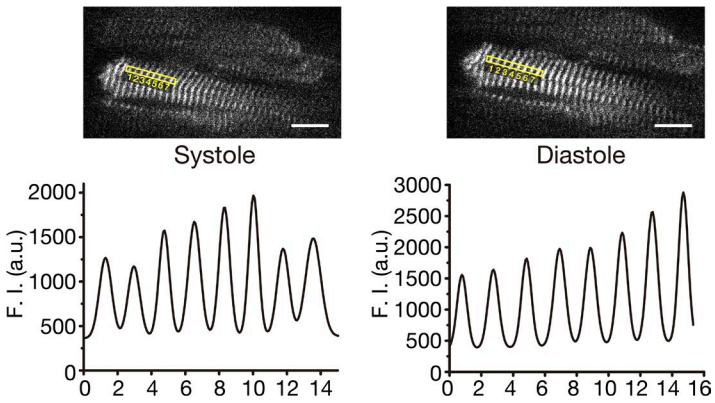

Figure S2. SL changes in the beating heart in vivo in a mouse showing high HR. (Top left) Confocal image of the myocyte in systole. Sarcomeres numbered from 1 to 7 were analyzed. (Bottom left) Plot profile along the longitudinal axis of the myocyte in top. SL, 1.75 ± 0.04 µm. (Top right) Confocal image of the myocyte in diastole. Sarcomeres numbered from 1 to 7 were analyzed (i.e., same as in left) because the image was in focus in this animal. (Bottom right) Plot profile along the longitudinal axis of the myocyte in top. SL, 1.99 ± 0.07 µm ($P < 0.05$ compared with the value in systole). Note clear striations in both systole and diastole at high HR. Measurements were made on an α-actinin–AcGFP-expressing myocyte in a mouse showing the highest HR value in Fig. 5 E (i.e., 523 bpm). Bar, 10 µm.

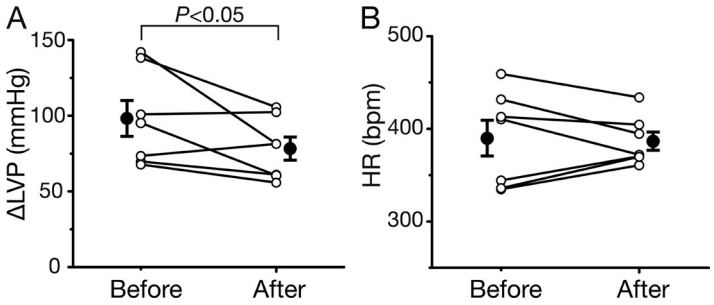

Figure S3. Changes in ΔLVP and HR after thoracotomy. (A) ΔLVP recorded before and after thoracotomy. Average values (closed circles), 98.2 ± 11.8 and 78.3 ± 7.7 mmHg before and after thoracotomy, respectively ($P < 0.05$). ΔLVP, difference in LVP in diastole and systole. (B) HR recorded before and after thoracotomy. Average values (closed circles), 390 ± 19 and 387 ± 10 bpm before and after thoracotomy, respectively ($P > 0.05$). Thin lines with open circles indicate the individual data. Number of animals, seven. Error bars represent mean± SEM.

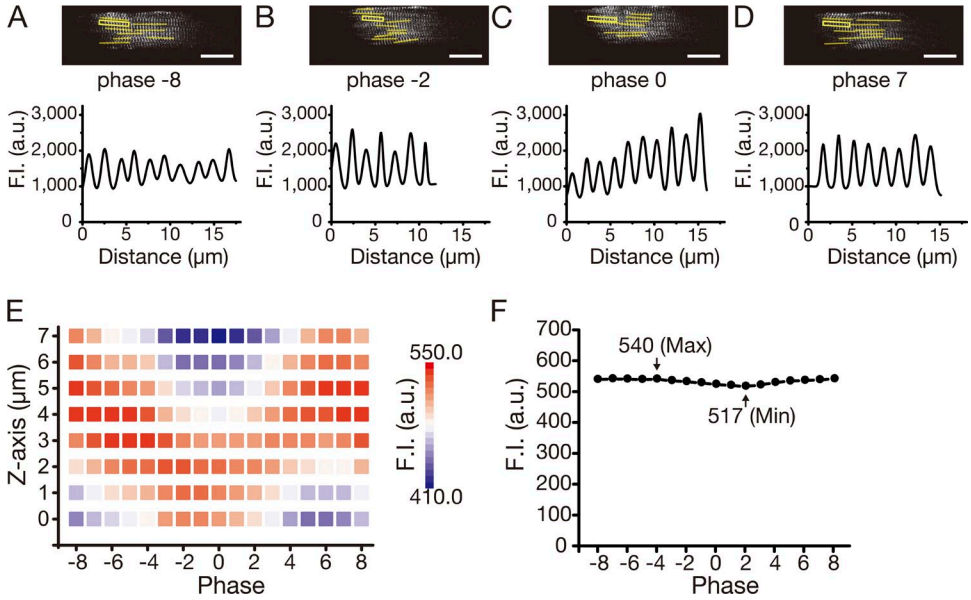

Figure S4. Sarcomeres in a myocyte in a beating heart in vivo with image sequence reconstruction. (A; top) Confocal image of the myocyte at phase −8, which is the same as that in Fig. 6 B, bottom. Bar, 20 μm. (Bottom) Plot profile of the yellow outlined rectangular region in the myocyte in top. SL, 1.76 ± 0.19 μm. (B; top) Confocal image of the myocyte at phase −2, which is the same as that in Fig. 6 B, bottom. Bar, 20 μm. (Bottom) Plot profile of the yellow outlined rectangular region in the myocyte in top. SL, 1.69 ± 0.12 μm ($P > 0.05$ compared with the value in A). (C; top) Confocal image of the myocyte at phase 0, which is the same as that in Fig. 6 B, bottom. Bar, 20 μm. (Bottom) Plot profile of the yellow outlined rectangular region in the myocyte in top. SL, 1.60 ± 0.08 μm ($P < 0.05$ compared with the value in A; $P > 0.05$ compared with the value in B). (D; top) Confocal image of the myocyte at phase 7, which is the same as that in Fig. 6 B, bottom. Bar, 20 μm. (Bottom) Plot profile of the yellow outlined rectangular region in the myocyte in top. SL, 1.73 ± 0.06 μm ($P < 0.05$ compared with the value in C; $P > 0.05$ compared with the value in A or B). Note that despite differing SL values, the images were in focus throughout the cardiac cycle, which is described in detail in Fig. 6 (compare Fig. 4 B). Length of the myocyte in the image plane, >50 μm throughout the cardiac cycle. Sarcomeres indicated by yellow lines were likewise used to derive the average SL values in Fig. 6 C. (E) Relation of phase (from −8 to 8; see Fig. 6) versus F.I. at various Z-directions (from 0 to 7 μm in the downward direction). F.I. obtained from an AcGFP-expressing myocyte (same as that in Fig. 6 B). Data represent average values obtained from 267 cardiac cycles. Pseudo colors used to indicate the level of F.I. Note that the Z-axis position varies as phase changes (∼5 μm in the transition from diastole to systole and vice versa). (F) Quantified graph showing maximal F.I. (along the Z-direction) at various phases (analyzed from E). In-focus images have greater numbers than defocused images because of high levels of AcGFP fluorescence. Note that the difference between the maximal and minimal values (shown by arrows) is less than ∼10%, showing the stability of F.I., despite the movement of the myocyte (see also A–D).

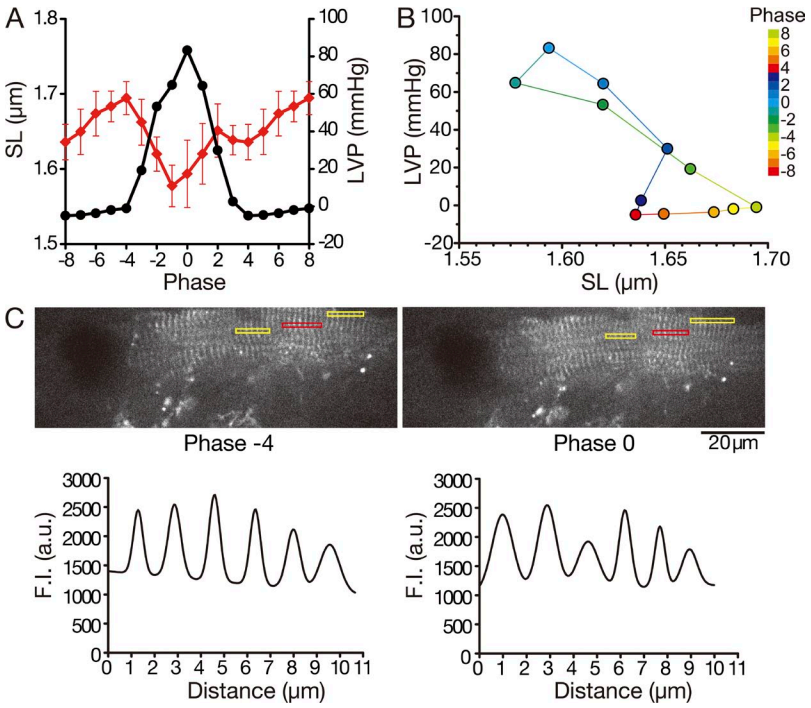

Figure S5. Cardiac sarcomere imaging with image sequence reconstruction in a mouse showing high systolic LVP. (A) Time-dependent changes in SL (red) and LVP (black) obtained from the reconstructed image sequence (as in Fig. 6 C). SL values were averaged at various phases from the reconstructed image sequence. LVP values were averaged at various phases from the data of 738 cardiac cycles. Error bars represent mean ± SEM. (B) Relationship between SL and LVP during the cardiac cycle. Average values of SL and LVP obtained in A were plotted. Colors indicate the phases in the cardiac cycle (as in right). (C; top) Confocal images of the myocyte at phase −4 (left) and 0 (right). Bar, 20 μm. Sarcomeres indicated by red and yellow outlined rectangular region were used to derive the average SL values in A and B. SL values were 1.66 ± 0.09 and 1.59 ± 0.24 μm at phases −4 and 0, respectively. (Bottom) Plot profile of the red outlined rectangular region in the myocyte in top. Despite differing SL values, the images were in focus throughout the cardiac cycle, at both phase −4 (∼0 mmHg) and 0 (∼80 mmHg).

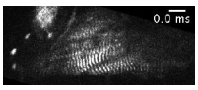

Video 1. Ventricular myocyte in the beating heart in vivo (without image sequence reconstruction). Cardiomyocyte expressing α-actinin–AcGFP located in the central part of the LV was imaged (see Fig. 4). Objective lens, 40× (N/A, 0.80; water immersion). Speed, 100 fps. Bar, 10 μm.

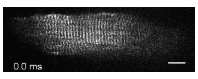

Video 2. Ventricular myocyte in the beating heart in vivo with image sequence reconstruction. Cardiomyocyte expressing α-actinin–AcGFP located in the central part of the LV was imaged (see Figs. 6B and S4, A–D). Objective lens, 60× (N/A, 1.00; water immersion). Speed, 100 fps. Bar, 10 μm.

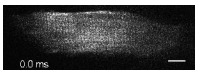

Video 3. Ventricular myocyte in the beating heart in vivo without image sequence reconstruction. Cardiomyocyte is the same as in Video 2. Note periodic defocused images as a result of movement of the heart. Objective lens, 60× (N/A, 1.00; water immersion). Speed, 100 fps. Bar, 10 μm.